



Geophysical Research Letters[®]



RESEARCH LETTER

10.1029/2022GL101003

Improving and Harmonizing El Niño Recharge Indices

Takeshi Izumo^{1,2}  and Maxime Colin^{3,4,5} 

Key Points:

- To clarify the debate on the Recharge Oscillator index, we develop an objective approach optimizing equation fit to observations
- The recharge index must be based on the slow component of sea level/thermocline depth, taken independently from the fast zonal tilt mode: this reconciles usual metrics
- The optimal index is this independent component averaged in the equatorial and southwestern Pacific. It is better suited for operational diagnostics

Supporting Information:

Supporting Information may be found in the online version of this article.

Correspondence to:

T. Izumo,
takeshi.izumo@ird.fr

Citation:

Izumo, T., & Colin, M. (2022). Improving and harmonizing El Niño recharge indices. *Geophysical Research Letters*, 49, e2022GL101003. <https://doi.org/10.1029/2022GL101003>

Received 24 AUG 2022

Accepted 14 OCT 2022

Author Contributions:

Conceptualization: Takeshi Izumo, Maxime Colin

Formal analysis: Takeshi Izumo

Investigation: Takeshi Izumo, Maxime Colin

Methodology: Takeshi Izumo, Maxime Colin

Validation: Takeshi Izumo, Maxime Colin

Visualization: Takeshi Izumo

Writing – original draft: Takeshi Izumo

Writing – review & editing: Takeshi Izumo, Maxime Colin

¹EIO, IRD-Iframer-UPF-ILM, Institut de Recherche pour le Développement (IRD), Université de la Polynésie Française (UPF), Tahiti, French Polynesia, ²Formerly at LOCEAN-IPSL, IRD, Sorbonne Université-CNRS-IRD-MNHN, Paris, France, ³Climate Change Research Centre, University of New South Wales (UNSW), Sydney, NSW, Australia, ⁴Laboratoire GEPASUD, University of French Polynesia (UPF), Tahiti, French Polynesia, ⁵Now at Leibniz Centre for Tropical Marine Research (ZMT), Bremen, Germany

Abstract El Niño Southern Oscillation (ENSO) is the leading mode of interannual climate variability, with large socioeconomical and environmental impacts. The main conceptual model for ENSO, the Recharge Oscillator (RO), considers two independent modes: the fast zonal tilt mode in phase with central-eastern Pacific Temperature (T_e), and the slow recharge mode in phase quadrature. However, usual indices (western or equatorial sea level/thermocline depth h) do not orthogonally isolate the slow recharge mode, leaving it correlated with T_e . Furthermore the optimal index is currently debated. Here, we develop an improved recharge index by objectively optimizing the RO equations fit to observations. (a) T_e -variability is regressed out, to build h_{ind} statistically-independent from T_e . Capturing the pure recharge, h_{ind} reconciles usual indices. (b) The optimum is equatorial plus southwestern Pacific $h_{\text{ind}_{\text{eq+sw}}}$ (because of ENSO Ekman pumping meridional asymmetry). Using $h_{\text{ind}_{\text{eq+sw}}}$, the RO becomes more consistent with observations. $h_{\text{ind}_{\text{eq+sw}}}$ is more relevant for ENSO operational diagnostics.

Plain Language Summary El Niño and La Niña events have important impacts globally. A key element for long-lead forecasts is the recharge state of the tropical Pacific Ocean, as captured in the Recharge Oscillator (RO) conceptual model. The RO considers two independent modes of oceanic variability, a fast adjustment process and a slow recharge/discharge process. However, usual recharge indices mix these two modes of variability, and can thus lead to ambiguous operational diagnostics of the actual oceanic recharge state. Here we develop a better recharge index, independent of the fast mode, which reconciles typical indices and allows us to go beyond the current geographical debate on the optimal metrics. We use an objective approach optimizing the RO resemblance to observations to find the optimal index: the independent sea level (or equivalently thermocline depth) averaged over the equatorial and southwestern tropical Pacific. We recommend this simple and unambiguous index for El Niño operational forecasts diagnostics.

1. Introduction

The El Niño Southern Oscillation (ENSO) is the leading mode of climate interannual variability, with large socioeconomic and environmental impacts (e.g., Clarke, 2008; Jin et al., 2020; Neelin et al., 1998; Timmermann et al., 2018; Wang and Picaut, 2004 reviews). While ENSO predictability skill is now rather good at short leads, it has to be improved at longer leads (e.g., Barnston et al., 2012, 2019). One key element for long-lead seasonal forecasts is the recharge state of the tropical Pacific (be it in terms of Oceanic Heat Content (OHC), thermocline depth h or sea level anomaly (SLA)), as it brings long oceanic memory across ENSO phases. Its role is formalized in the Recharge Oscillator (RO) conceptual model of ENSO (e.g., Clarke, 2010; Clarke et al., 2007; Jin, 1997a, 1997b; Wyrski, 1985). For example, during a La Niña, easterlies favor a slow accumulation of OHC in the western and equatorial Pacific. This recharge will progressively favor positive Sea Surface Temperature (SST) anomalies in the central-eastern equatorial Pacific (T_e) and thus El Niño onset through the Bjerkness positive feedback. The El Niño event will in turn lead to a discharge favoring a reversal to La Niña conditions. The RO can thus well explain ENSO cyclic nature (cf. Section 3 for RO equations).

Yet there is a debate on the best recharge metric, for example, western or equatorial Pacific, sea level or thermocline depth. In the RO, the equatorial Pacific basin adjustment is separated into two independent modes: (a) the fast adjustment mode associated to a zonal tilt of the thermocline, in phase with zonal equatorial wind stress τ_x and T_e (Figure 1a); (b) the slow adjustment recharge mode in phase quadrature with the fast mode (and thus with τ_x and T_e ; Figure 1b). Several indices have been developed for this slow recharge mode that all bring predictability

© 2022. The Authors.

This is an open access article under the terms of the [Creative Commons Attribution License](https://creativecommons.org/licenses/by/4.0/), which permits use, distribution and reproduction in any medium, provided the original work is properly cited.

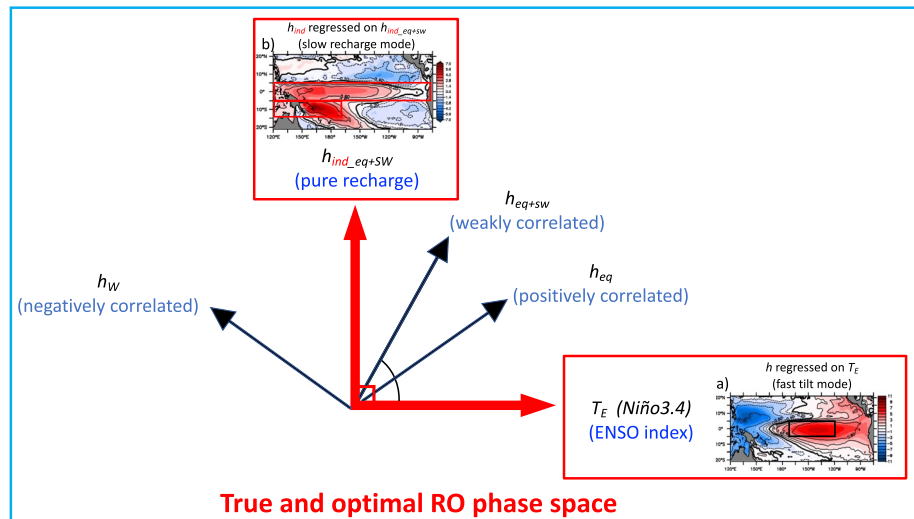


Figure 1. Schematics of the optimal orthonormal phase space for the Recharge Oscillator (RO). Panels a and b show respectively the fast adjustment zonal tilt mode dependent of T_E (h regressed onto T_E , i.e., K) and the pure recharge mode (h_{ind} regressed onto our default best recharge index h_{ind_eq+sw}), independent of (uncorrelated to) T_E (h unit: satellite SLA in cm; c.f. Sections 1 and 3 for details). Black arrows illustrate other used indices based on usual h . They are hence partly correlated to T_E .

skill. Wyrski (1985) and Jin (1997a, 1997b) originally focused on the western equatorial Pacific h_w , using equivalently SLA, OHC or the actual thermocline depth for h . Jin's sketch, Meinen and McPhaden (2000), and Burgers et al. (2005) focused on the mean equatorial band: h_{eq} (e.g., Warm Water Volume (WWV) based on the 20°C isotherm depth Z20, or SLA, as usual thermocline depth proxies). h_{eq} has become a widely-used ENSO recharge index. Theoretically, in the RO model, h_{eq} is independent (i.e., uncorrelated at lag 0) from the fast tilt mode (and thus from T_E) within Jin (1997a, 1997b) approximations.

This independence/orthogonality property is essential, so that the recharge metric captures solely the *pure* recharge mode and does not mix it with the fast adjustment mode. But in observations, h_{eq} (and its proxies) is not independent (Figure 1; upper-right panel of Figure S2 in Supporting Information S1). It is physically ambiguous, mixing the fast adjustment with the slow recharge mode, and thus potentially misleading: h_{eq} is dominated by a short-term Ekman convergence leading to a temporary *fast* “increase” with *El Niño westerlies* (thus not a true long-term recharge in the RO sense), about two times larger (for SLA-based h_{eq}) than the long-term *slow discharge* expected from the RO theory. h_{eq} is hence first an index of the fast equatorial Kelvin wave rather than of the RO long-term recharge/discharge process (Izumo, Lengaigne, et al., 2018; see also Neske and McGregor, 2018). Thus h_{eq} is strongly positively correlated to the fast mode (and thus to τ_x and T_E). Hence, Izumo, Lengaigne, et al. (2018) recommended the use of a western Pacific index, h_w (in agreement with Ballester, Petrova, et al., 2016; Boschat et al., 2013; Graham et al., 2015; Jin et al., 2020; Lai et al., 2015; Ramesh and Murtugudde, 2013; Petrova et al., 2017). Yet, such western Pacific OHC index is also not independent of T_E . It is partly negatively correlated to the fast zonal tilt mode (Figure 1a). h_w could thus also lead to ambiguous diagnostics of the actual oceanic state.

Therefore the fast adjustment mode needs to be removed in order to obtain an operationally-useful indicator of the fully-isolated recharge process. Here we will hence develop an improved recharge index h_{ind} independent of the fast mode. We will show that previously-defined indices converge when using h_{ind} . We will develop an objective approach optimizing the skill of the RO differential equations fit to observations for the (T_E, h_{ind}) pair to find the optimal averaging region for h_{ind} : h_{ind_eq+sw} .

2. Data and Methods

Here we use classical observations and reanalyzes datasets, indices and statistical methods, detailed in Text S1 in Supporting Information S1 (statistics robust thanks to a sufficiently-large number of effective degrees of freedom, ~ 85 to ~ 140). The ENSO index T_E is Niño3.4 relative Sea Surface Temperature (RSST, i.e.,

SST minus its 20°N–20°S tropical mean), as recommended by Izumo et al. (2020) and Van Oldenborgh et al. (2021) because atmospheric tropical deep convection interannual anomalies are rather related to RSST than to SST. Theoretically, SST is the variable directly involved for the term $F_1 * h$ in the dT_E/dt equation (cf. Section 3). Yet, the recharge process is driven by windstress, itself directly driven by atmospheric deep convection and thus by RSST. Therefore, Niño3.4 RSST is better for the term $F_2 * T_E$ in the dh/dt equation (Text S3 in Supporting Information S1). Using SST instead of RSST, or Niño3 instead of Niño3.4, makes T_E slightly less correlated to equatorial Pacific τ_x (i.e., ocean-atmosphere coupling), but leads to very similar results (Table S2 in Supporting Information S1).

3. Improving the Recharge Oscillator Recharge Index

3.1. Traditional RO Framework Revisited

To derive RO dT_E/dt tendency equation (see Jin et al., 2020 review for derivation), some physically-reasonable assumptions are used. (a) τ_x is proportional to T_E , that is, tropical deep convection and related τ_x respond quickly to T_E . (b) The fast oceanic response (i.e., quasi-instantaneous, timescales faster than ~ 2 – 3 months) to τ_x leads to a positive Bjerkness feedback term in the dT_E/dt equation (through both the zonal advective and thermocline feedbacks) that is proportional to τ_x and thus to T_E : $R_{BJ,o} T_E$. (c) Atmospheric fluxes are approximated as a weak Newtonian damping proportional to T_E : $-r_{damp,o} T_E$. (d) A deepening of the thermocline depth h related to a recharge favors positive T_E on time scales longer than 2–3 months: $F_1 h$ (see Text S2 in Supporting Information S1 on mechanisms). Therefore:

$$\frac{dT_E}{dt} = R_o T_E + F_1 h \quad (1)$$

the first term on the right hand side representing the net effect of Bjerkness positive feedback and Newtonian damping ($R_o = R_{BJ,o} - r_{damp,o}$) and the second one, F_1 , the recharge/discharge influence on T_E (following Jin et al., 2020 notations).

Concerning dh/dt equation, in the RO, the slow recharge mode response is the temporal integral of τ_x (e.g., Izumo et al., 2014). Negative T_E associated with easterly anomalies will progressively recharge the equatorial Pacific (see Section 3.3 and Text S2 in Supporting Information S1). This is formalized as a term $-F_2 T_E$ in the dh/dt equation:

$$\frac{dh}{dt} = -F_2 T_E - \epsilon_o h \quad (2)$$

the second term $-\epsilon_o h$ being formally a Newtonian damping, expected to be weak.

That is, the tendency equation for the vector $\begin{pmatrix} T_E \\ h \end{pmatrix}$ in matrix form is:

$$\frac{d}{dt} \begin{pmatrix} T_E \\ h \end{pmatrix} = \begin{pmatrix} R_o & F_1 \\ -F_2 & -\epsilon_o \end{pmatrix} \begin{pmatrix} T_E \\ h \end{pmatrix} \quad (3)$$

This RO linear equation is simple, but it remains unclear which geographical box to use for h . Furthermore, a standard multivariate linear regression fit minimizing rms error (second method in Burgers et al., 2005) gives significantly different coefficients for the classical normalized metrics h_w and h_{eq} : $R_o = \epsilon_o = +0.06 \pm 0.04$ and -0.18 ± 0.05 months $^{-1}$ for h_w and h_{eq} respectively, $F_1 = F_2 = 0.15 \pm 0.04$ and 0.25 ± 0.05 months $^{-1}$ respectively. The fact that R_o and ϵ_o can change sign so easily for different classical recharge metrics makes it hard to interpret them physically. It evidences some physical inconsistency (Figure 1).

To resolve these geographical debate and physical issues objectively, an empirical way to find the best h is to have no a priori on the best region and index. Thus, one may intuitively think of searching for the $h(x, y, t)$ region that statistically optimizes the skill of Equation 3. We will actually show later that we need two steps to construct

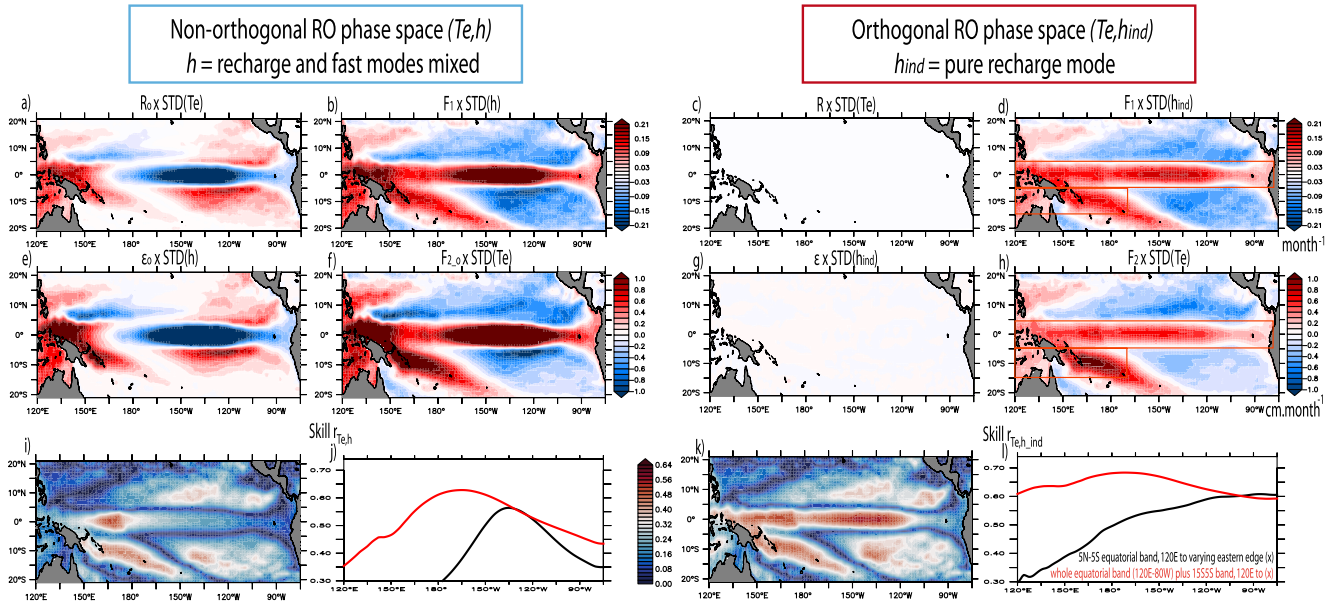


Figure 2. Searching for the optimal recharge index h , representing the actual slow recharge mode independent of the fast mode in RO equations. Usual non-orthogonal basis (T_E, h) in the left set of panels, and orthogonal basis (T_E, h_{ind}) in the right one. Panels a and b show respectively the coefficients $R_0(x, y)$ and $F_1(x, y)$ for the multivariate regression of $dT_E/dt(t)$ onto $T_E(t)$ and $h(x, y, t)$ (Equation 4), multiplied by the STDs of $T_E (=1)$ and of $h(x, y, t)$ respectively, to measure their respective contributions to $dT_E/dt(t)$. Panels e and f are as a and c, but for coefficients for $dh(x, y, t)/dt$ regression. Panel i shows $r_{Te,h}$ skill using $h(x, y, t)$. Black line in panel j shows this skill for h averaged over: the equatorial band (5°N – 5°S) with its western edge fixed to 120°E and its eastern edge varying, given by the x -axis. Red line is for a two-rectangle region, the classical equatorial box (5°N – 5°S , 120°E – 80°W) plus a southern 5°S – 15°S box with the same 120°E fixed western edge and its eastern edge varying. The right set of panels is the same for the here-developed orthogonal basis (T_E, h_{ind}) . The boxes overlaid represents the two-rectangle equatorial + SouthWest ($eq + sw$) optimal region finally chosen to average h_{ind} . This defines the suggested improved index: h_{ind_eq+sw} . See text for details.

a better index: (a) independence to T_E , (b) geographical optimization of the averaging region. Let us first try the geographical optimization alone:

$$\frac{d}{dt} \begin{pmatrix} T_E(t) \\ h(x, y, t) \end{pmatrix} = \begin{pmatrix} R_0(x, y) & F_1(x, y) \\ -F_{2_0}(x, y) & -\epsilon_0(x, y) \end{pmatrix} \begin{pmatrix} T_E(t) \\ h(x, y, t) \end{pmatrix} + \begin{pmatrix} \text{residual}_T(x, y, t) \\ \text{residual}_h(x, y, t) \end{pmatrix} \quad (4)$$

In practice we do at each spatial point (x, y) a fit with two multivariate linear regressions, one for Equation 1 and one for Equation 2, with Pearson correlation skill r_{Te} and r_h respectively. The squareroot of the RV-coefficient (Rho-Vectoriel; Escoufier & Robert, 1976), “ $r_{Te,h}$,” is the equivalent of the Pearson correlation for matrix form, that is, a measure of the skill for the 2D Equation 4. Where the skill is the highest (residuals variance minimized) should inform us of the best h region to capture the RO processes. The highest skill is in the equatorial and south-western tropical Pacific (Figure 2i), suggesting that the best region for averaging $h(x, y, t)$ could combine these two regions. However, the regression coefficients contributions have a puzzling spatial distribution (Figures 2a, 2b, 2e, and 2f). They are highly spatially-correlated with large opposing signs. In the central Equatorial Pacific, T_E and h influences on dT_E/dt would be very large, but negative for R_0 and positive for F_1 respectively, which is unphysical. This is actually a statistical artifact because $T_E(t)$ and $h(x, y, t)$ are not statistically independent (i.e., not orthogonal), which makes it difficult to interpret physically the regression coefficients. It therefore suggests that the (T_E, h) basis is not ideal.

3.2. Toward New RO Tendency Equations for T_E and Independent h_{ind}

A large component of h responds rapidly to τ_x and T_E . This fast response component of h is correlated to (i.e., linearly dependent of) T_E at timescales longer than ~ 2 – 3 months in the equatorial Pacific: Figure 1a shows the downwelling pattern along the central to eastern equatorial Pacific and the zonal seesaw pattern in the western Pacific, that is, the fast adjustment mode. We suggest to regress out from $h(x, y, t)$ this rapidly-responding component correlated to $T_E(t)$, so as to only focus on the slowly-responding independent component of h , hereafter h_{ind}

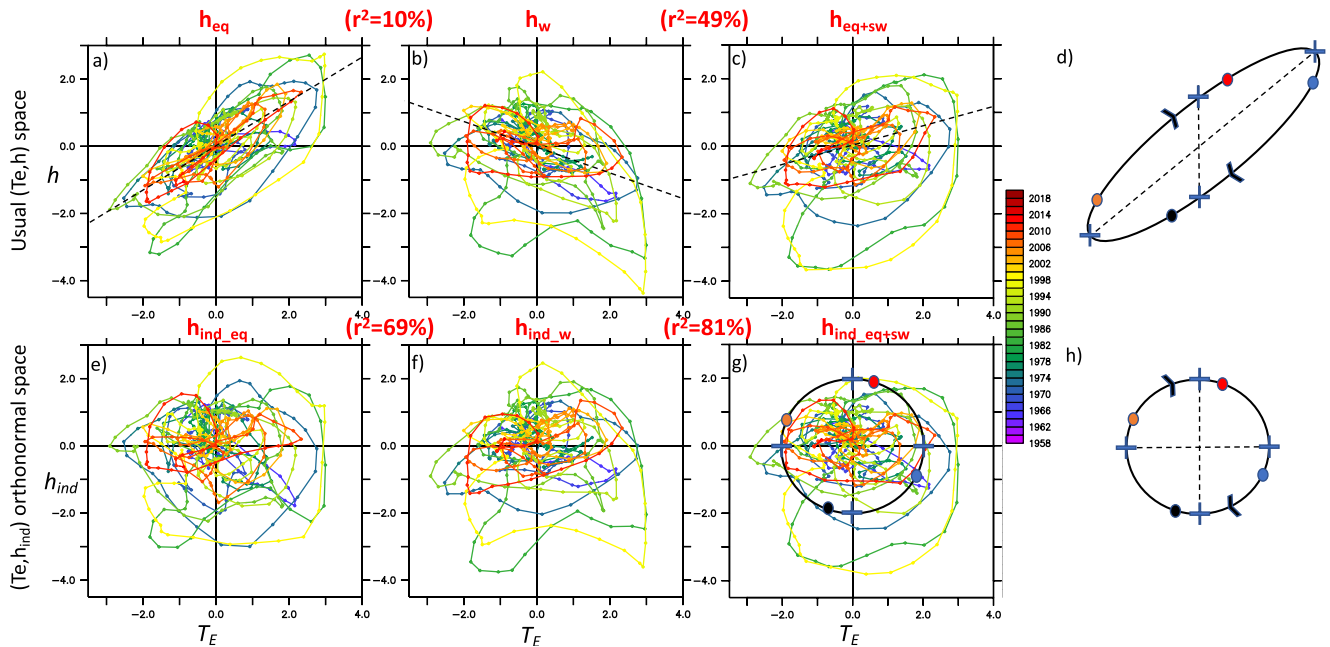


Figure 3. Observed trajectories of the RO in the usual (T_E, h) space (upper panels) and new orthonormal (T_E, h_{ind}) space (lower panels), for classical h_{eq} and h_w indices (1st and 2nd columns), and optimal h_{eq+sw} index (3rd column). (a) Trajectory of the system for the pair of coordinates (T_E, h_{eq}) , T_E in horizontal axis, h in vertical axis, each month being a point, with year indicated in color, for ORAS5 SLA. Other panels are similar, but for other recharge indices. Indices are all normalised. The shared variance (square of correlation) between recharge indices is shown in parenthesis. (d) schematized elliptical trajectory if the recharge index is positively correlated to T_E , such as h_{eq} . Such index is ambiguous. For example, a positive anomaly does not necessarily correspond to an actual recharge state (blue dot). (h) circular trajectory for the recharge index independent component, consistent with ideal RO trajectory, and unambiguous. Color dots indicate different positions in the cycle.

(Figure 3b of Izumo, Lengaigne, et al., 2018). h_{ind} corresponds to the slow recharge mode related to the slower basin adjustment in disequilibrium with wind stress (e.g., Alory & Delcroix, 2002; Clarke, 2010; Fedorov, 2010; Jin, 1997a, 1997b; Masuda et al., 2009; Thual et al., 2013; Zhu et al., 2017; Izumo, Lengaigne, et al., 2018). Thus, we can formally decompose h :

$$h(x, y, t) = h_{fast_mode(dependent, corr. to T_E)} + h_{slow_recharge_mode(independent, uncorr. to T_E)}$$

$$h(x, y, t) = K(x, y) T_E(t) + h_{ind}(x, y, t) \quad (5)$$

$K(x, y)$ being the regression coefficient of h onto T_E (Figure 1a).

h_{ind} is the pure recharge component, that allows us to describe the system with an orthonormal basis: (T_E, h_{ind}) (Figure 1). An orthonormal basis is more acceptable physically and mathematically.

With this linear transform, Equation 4 can then be rewritten as:

$$\frac{d}{dt} \begin{pmatrix} T_E(t) \\ h_{ind}(x, y, t) \end{pmatrix} = \begin{pmatrix} R(x, y) & F_1(x, y) \\ -F_2(x, y) & -\varepsilon(x, y) \end{pmatrix} \begin{pmatrix} T_E(t) \\ h_{ind}(x, y, t) \end{pmatrix} + \begin{pmatrix} residual_T(x, y, t) \\ residual_{h_{ind}}(x, y, t) \end{pmatrix} \quad (6)$$

with $R = R_o + K F_1$, $F_2 = F_{2,o} + \varepsilon_o K + K R_o + K^2 F_1$, $\varepsilon = \varepsilon_o + K F_1$ and $residual_{h_{ind}} = residual_h - K residual_T$.

So the F_1 term representing the recharge influence on T_E remains the same for h_{ind} , and the physics behind is also the same. F_2 represents the influence of easterly anomalies related to T_E on the h_{ind} recharge. It differs from $F_{2,o}$.

Figures 2c, 2d, 2g, and 2h show the coefficients obtained from the multivariate regression onto (T_E, h_{ind}) . R and ε are uniformly negligible ($\sim 0.00 \pm 0.03$ months $^{-1}$). F_1 and F_2 vary spatially similarly, with highest values in the equatorial and southwest Pacific corresponding to the highest skill (Figure 2k and Figure S1 in Supporting Information S1). Hence the best h_{ind} region should combine these two regions. The picture is also clearer and more consistent with RO theory: ε is negligible, consistent with a weak damping (due mainly to oceanic mixing,

e.g., Fedorov, 2010). $r_{T_E, h_{ind}}$ is larger than $r_{T_E, h}$ (Figure 2i), further confirming that (T_E, h_{ind}) is a better basis of RO phase space.

Here we explain the spatial patterns of Figure 2's various panels (full explanation in Text S2 in Supporting Information S1), robust among datasets and periods (cf. Figure S2 in Supporting Information S1), and why there are similarities among some of them. F_2 map shows us how $h_{ind}(x, y, t)$ would look like if ENSO windstress anomalies would blow for a long time, for example, because of long-lasting La Niña conditions. The slow recharge is as expected in the western and central equatorial Pacific, through: (a) downwelling equatorial Rossby waves to the west (Jin, 1997a, 1997b; Wyrтки, 1985), and off-equatorial ones in the southwest; (b) upwelling equatorial Kelvin waves to the east forcing coastal Kelvin waves propagating poleward along the eastern boundary and thus leading to a leakage of negative OHC anomalies toward the poles along the eastern boundary (Izumo, Lengaigne, et al., 2018; Wyrтки, 1985).

Interestingly the recharge is also in the southwest, because of asymmetric Ekman pumping (poleward shift of the South Pacific Convergence Zone; SPCZ) forcing locally downwelling (in the La Niña case) and thus slow off-equatorial downwelling Rossby waves progressively recharging the southwestern Pacific. Note that the western boundary coastline meridional asymmetry would conversely favor a larger northwest recharge, as shown by sensitivity experiments with the LCS model (Linear Continuously Stratified model; McCreary, 1980; configuration of Izumo, Lengaigne, et al., 2018; Figure S3 in Supporting Information S1). F_1 physically represents the slow recharge mode influence on T_E through several mechanisms (Text S2 in Supporting Information S1).

R_o , ϵ_o and $F_{2,o}$ spatial patterns can be explained as follow: $R_o \approx \epsilon_o \approx -KF_1$ and $F_{2,o} \approx F_2 + K^2F_1$ (as $\epsilon \approx 0$ and $R \approx 0$). These relationships explain the paradox (pointed out in Section 3.1) with large positive and negative R_o and ϵ_o values found for classical h_w and h_{eq} respectively: $R_o \approx \epsilon_o > 0$ (because $K < 0$ in the west) for h_w and $R_o \approx \epsilon_o < 0$ (because $K > 0$) for h_{eq} , even if the actual damping ϵ and net feedback R are weak. So the “damping” term (ϵ_o) and the “positive feedback” (R_o) would be artificially large. This further confirms that we should use h_{ind} rather than the full h polluted by the fast mode that biases the RO model.

Such transforms from observable variables to new variables that are more relevant physically are often done in physics and geosciences, for example, to create potential temperature, relative SST, rotating PCs (Takahashi et al., 2011), decomposition into baroclinic modes, spherical harmonics... We just want to clearly isolate the independent influence of the slow recharge mode from the fast tilt mode, and to optimize the RO understanding and metrics (we are not trying to add new physical processes).

Considering h_{ind} instead of h allows us to go beyond the RO metrics debate, by reconciling indices: they become much closer when considering their independent component. For example, h_{ind_w} and $h_{ind_{eq}}$ are much better correlated (r^2 increases from 10% to 69%) with now similar coefficients (Figures S4, S5 and Table S2 in Supporting Information S1). And Z20 and SLA-based indices become even closer (Figure S6 in Supporting Information S1). Trajectories in the (T_E, h_{ind}) phase diagram (Dommenget & Al-Ansari, 2022; Kessler, 2002) also become closer (Figure 3; shown here for longer ORAS5 SLA data set to have a larger density; see Figures S7 and S8 in Supporting Information S1 for satellite SLA and ORAS5 Z20). The transform is geometrically simply a linear transform of coordinates from the (T_E, h) to the (T_E, h_{ind}) orthogonal coordinate space. Trajectories in the latter space are more circular, closer to idealized RO model circular trajectory.

To conclude, h_{ind} reconciles various recharge metrics such as h_{ind_w} and $h_{ind_{eq}}$. Here below we would like to further improve them by objectively finding h_{ind} optimal averaging region.

3.3. Objectively Finding the Optimal Region: Equatorial + South-West ($h_{ind_{eq+sw}}$)

The optimal region for $h_{ind}(x, y, t)$ will be the one optimizing the skill $r_{T_E, h_{ind}}$ of the RO tendency Equation 6

for $\begin{pmatrix} T_E \\ h_{ind} \end{pmatrix}$:

$$\frac{d}{dt} \begin{pmatrix} T_E \\ h_{ind} \end{pmatrix} = \begin{pmatrix} R & F_1 \\ -F_2 & -\epsilon \end{pmatrix} \begin{pmatrix} T_E \\ h_{ind} \end{pmatrix} \quad (7)$$

$r_{Te,h_{ind}}$ (Figure 2k) is the largest in the equatorial ($\sim 5^{\circ}\text{N}$ – 5°S) and southwest ($\sim 5^{\circ}\text{S}$ – 15°S) Pacific. The combination of these two boxes should be our optimal region, and $r_{Te,h_{ind}}$ should be even better thanks to the spatial averaging (reducing noise). To choose objectively the optimal averaging region, we have tested several options. We have first tested rectangular boxes, for example, by averaging $h_{ind}(x, y, t)$ from the usual fixed 120°E western end to a varying eastern edge, for various latitudinal bands. For the classical 5°N – 5°S band, the best skill ($r_{Te,h_{ind}} = 0.61$) is found for an eastern edge around ~ 90 – 80°W (Figure 2l, black line), consistent with classical h_{eq} (5°N – 5°S , 120°E – 80°W). Another relevant band is the 5°N – 15°S , 120°E to $\sim 150^{\circ}\text{W}$, leading to a similarly high skill (not shown). A “hybrid” choice with two rectangles is even better. Adding to the optimal classical equatorial band (5°N – 5°S , 120°E – 80°W) a second box in the southwest, along the 5°S – 15°S band, from the same 120°E western edge to a varying eastern edge, further improves the skill to $r_{Te,h_{ind}} = 0.69$ for an optimal eastern edge around $\sim 170^{\circ}\text{W}$ (Figure 2l, red line). We have similarly tested all the other edges of this two-rectangle region, also testing ORAS5 SLA and Z20 (Figures S9a, S9b, and S10 in Supporting Information S1). This is our best allround and sufficiently-simple index, hereafter $h_{ind_{eq+sw}}$ (note that $h_{ind_{eq+sw}} = h_{eq+sw_{ind}}$, the regression being linear). Interestingly, this choice also conveniently minimizes the correlation between h_{eq+sw} and T_E (Figures S9c and S9d in Supporting Information S1), making h_{eq+sw} closer to $h_{ind_{eq+sw}}$. The skill increase from $h_{ind_{eq}}$ to $h_{ind_{eq+sw}}$ is statistically significant, more thanks to $r_{h_{ind}}$ ($p = 0.0110.00110.001$) than to r_{Te} ($p = 0.0910.0110.23$) for satSLA|ORAS5_SLA|ORAS5_Z20 respectively). And trajectories are even smoother (Figure 3g). Including the southwest agrees with Izumo et al. (2018a; see also Santoso et al., 2017; Ramesh and Murtugudde, 2013). $h_{ind_{eq+sw}}$ is now our default best recharge index.

Using normalized $h_{ind_{eq+sw}}$, we obtain: $F_1 \approx F_2 \approx 0.17 \pm 0.03$, $R \approx \varepsilon \approx 0.00 \pm 0.03 \text{ months}^{-1}$. These coefficients are robust among datasets and periods (Table S1 in Supporting Information S1). R and ε are negligible. This reduces the parameter space. And the RO equations system has the form of a harmonic oscillator excited by noise (Burgers et al., 2005), with $d^2X(t)/dt^2 \approx -F_1F_2X(t)$, $X(t)$ being T_E or h_{ind} , and angular frequency being the Wyrтки index $W = (F_1F_2)^{1/2} \approx F_1 \approx F_2$ (i.e., reasonable eigenperiod of ~ 3.1 year). Even if theoretically undamped, the oscillator is actually still damped because $residual_T$ is not a pure red noise but includes non-linear terms neglected in our first order linear approximation (Table S2 in Supporting Information S1).

4. Conclusion

4.1. Summary

Here we have defined a simple Pacific recharge index h_{ind} independent of the fast mode, by regressing out T_E -related variability. It unambiguously represents the slow recharge mode, with more physically-consistent RO parameters, conversely to classical recharge indices. h_{ind} harmonizes recharge indices: by taking h_{ind} , averages over the usual western/equatorial Pacific regions based on Z20/OHC/SLA have much more similar time series, equation parameters and phase trajectories, so that all indices converge to a single one. We have also objectively searched for the optimal averaging region to have the most realistic RO tendency equations. The optimal index is $h_{ind_{eq+sw}}$ averaged over the classical equatorial band (5°N – 5°S , 120°E – 80°W), extended in the southwest until 15°S (5°S – 15°S , 120°E – 170°W).

In practice, obtaining $h_{ind_{eq+sw}}$ is straightforward: (a) average SLA over “eq + SW” box and then normalize, (b) remove its dependent part KT_E : $h_{ind_{eq+sw}} = h_{eq+sw} - K_{eq+sw}T_E$, with regression coefficient $K_{eq+sw} \approx 0.26$ (details in Text S1 in Supporting Information S1).

4.2. Discussion

For ENSO operational diagnostics, the $(T_E, h_{ind_{eq+sw}})$ basis is more relevant to describe the system trajectory than the usual (T_E, h_{eq}) and (T_E, h_w) pairs (Figure 3). If the latter are used, a situation with anomalous h is ambiguous. Independent $h_{ind_{eq+sw}}$ better represents actual precursory recharge anomalies. Only with h_{ind} sign (recharged/discharged state) can one get dT_E/dt sign directly (while h sign is not sufficient, as the fast tilt mode signal could blur a weaker long-term build-up; see yellow/blue dots in idealized schematics Figures 3d and 3h).

To compare $h_{ind_{eq}}$ and $h_{ind_{eq+sw}}$ forecasting skills, we have done a preliminary assessment by using the simple multivariate linear regression model combining the recharge index, Indian Ocean Dipole (IOD) index and T_E , all in September–November, to hindcast T_E peak in November–January 14 months later. Adding the Southwest

improves the skill for all datasets/periods, more clearly for SLA than for Z20 (Table S3 in Supporting Information S1; since we have statistically-significant contributions from $h_{\text{ind_eq} + \text{sw}}$ and IOD, but not from T_E itself, this new recharge index and updated datasets confirm earlier studies of Izumo et al., 2010, 2014, 2016; Dayan et al., 2014; Jourdain et al., 2016).

Results are robust among datasets. Only some subtle second order differences remain between SLA and Z20 (OHC being inbetween) for h_{ind} , likely related to different weighting of the first baroclinic modes (Figures S2, S6, S8, and S10 in Supporting Information S1). Note that we are not trying to address “how to best estimate the thermocline depth” (Vijayeta et al., 2020), but rather “how to best isolate the recharge mode.” SLA and Z20 each have their own advantages with presently-available datasets: Z20 seems better in a perfectly-observed and non-warming ocean (Tables S1 and S3 in Supporting Information S1), but SLA is observed globally by satellite in near real-time and is more available in climate models outputs (e.g., Coupled Model Intercomparison Project, CMIP).

Here we have neglected possible seasonal cycles of parameters and asymmetries/non-linearities for the sake of simplicity. Knowing ENSO seasonal phase-locking, taking into account such seasonal cycles could be one next step. We could include asymmetrical/non-linear terms (Table S2 in Supporting Information S1). To have a simple h_{ind} definition, we have also neglected a weak non-linearity in the fast response of h to T_E (Figure 3c; Figures S7c and S8c in Supporting Information S1) likely due to τ_x anomalies longitudinal position, further to the east during El Niño than during La Niña, favoring a larger discharge. This non-linearity would lead to a quadratic term in the dh_{ind}/dt equation.

Our method is based on a statistical optimisation of regression coefficients from observations to fit the RO model, by projecting on an orthogonal basis, which is conceptually satisfying, and practically necessary to determine eigenmodes. But correlations do not mean causality, and this study therefore does not aim to challenge RO physical validity. Although using the physical h variable is necessary to infer causality and derive RO equations, we still argue that having orthogonal coordinates thanks to h_{ind} allows for clearer recharge diagnostics, and a properly isolated recharge mode.

Some studies, using usual h indices, have put in question the RO and suggested that the delayed oscillator (DO, Suarez and Schopf, 1988; Battisti & Hirst, 1989) is more realistic (e.g., Graham et al., 2015; Linz et al., 2014). One reason for this “RO versus DO” debate could be the misleading character of usual h indices because of fast tilt mode (dependent) component, which tends to artificially reduce RO skill. It would be interesting to compare the RO to the other ENSO oscillators, using $h_{\text{ind_eq} + \text{sw}}$ instead, to clarify whether theories, climate models and observations would better agree.

Acknowledgments

MC would like to thank Steven Sherwood for his essential support, supervision, and mentoring, in particular throughout the pandemic, which made this collaboration possible. We would like to thank the two reviewers, notably Dr. Dietmar Dommenget for his critical thinking and interesting discussions, who have pushed us to improve, clarify and strengthen the results, as well as Dr. Matthieu Lengaigne, Dr. Jérôme Vialard, and Pr. Fei-Fei Jin for discussions. T.I. and M.C. would like to thank UPF for hosting M.C. because of COVID-related closed Australian borders; this latter fact was paradoxically essential for allowing us to make this work mature. We also thank UNSW Sydney for allowing a flexible work agreement for MC during the pandemic. M. Colin was first supported by the Australian ARC Grant FL150100035 and kindly hosted by UPF, and then directly funded by the ZMT's core budget. T. Izumo was funded mainly by IRD core budget, with some funding from ANR ARISE project.

Data Availability Statement

All data used is open data: OISSTv2 (<https://psl.noaa.gov/data/gridded/data.noaa.oisst.v2.html>), CMAP1 (<https://psl.noaa.gov/data/gridded/data.cmap.html>), ERA5-ORAS5 (<https://www.ecmwf.int>), Copernicus SLA (<https://doi.org/10.48670/moi-00148>), and HadISST (<https://www.metoffice.gov.uk/hadobs/hadisst/>). We acknowledge use of NOAA pyferret open source software for analyses and figures.

References

- Alory, G., & Delcroix, T. (2002). Interannual sea level changes and associated mass transports in the tropical Pacific from TOPEX/Poseidon data and linear model results (1964–1999). *Journal of Geophysical Research*, 107(C10), 17–21. <https://doi.org/10.1029/2001jc001067>
- Ballester, J., Petrova, D., Bordoni, S., Cash, B., García-Díez, M., & Rodó, X. (2016). Sensitivity of El Niño intensity and timing to preceding subsurface heat magnitude. *Scientific Reports*, 6(1), 1–9. <https://doi.org/10.1038/srep36344>
- Barnston, A. G., Tippett, M. K., L'Heureux, M. L., Li, S., & DeWitt, D. G. (2012). Skill of real-time seasonal ENSO model predictions during 2002–11: Is our capability increasing? *Bulletin of the American Meteorological Society*, 93(5), 631–651. <https://doi.org/10.1175/bams-d-11-00111.2>
- Barnston, A. G., Tippett, M. K., Ranganathan, M., & L'Heureux, M. L. (2019). Deterministic skill of ENSO predictions from the North American multimodel ensemble. *Climate Dynamics*, 53(12), 7215–7234. <https://doi.org/10.1007/s00382-017-3603-3>
- Battisti, D. S., & Hirst, A. C. (1989). Interannual variability in a tropical atmosphere–ocean model: Influence of the basic state, ocean geometry and nonlinearity. *Journal of the Atmospheric Sciences*, 46(12), 1687–1712. [https://doi.org/10.1175/1520-0469\(1989\)046<1687:iviata>2.0.co;2](https://doi.org/10.1175/1520-0469(1989)046<1687:iviata>2.0.co;2)
- Boschat, G., Terray, P., & Masson, S. (2013). Extratropical forcing of ENSO. *Geophysical Research Letters*, 40(8), 1605–1611. <https://doi.org/10.1002/grl.50229>
- Burgers, G., Jin, F.-F., & van Oldenborgh, G. J. (2005). The simplest ENSO recharge oscillator. *Geophysical Research Letters*, 32(13), L13706. <https://doi.org/10.1029/2005GL022951>

- Clarke, A. J. (2008). *An introduction to the dynamics of El Niño and the southern oscillation*. Elsevier.
- Clarke, A. J. (2010). Analytical theory for the quasi-steady and low-frequency equatorial ocean response to wind forcing: The “tilt” and “warm water volume” modes. *Journal of Physical Oceanography*, *40*(1), 121–137. <https://doi.org/10.1175/2009jpo4263.1>
- Clarke, A. J., Van Gorder, S., & Colantuono, G. (2007). Wind stress curl and ENSO discharge/recharge in the equatorial Pacific. *Journal of Physical Oceanography*, *37*(4), 1077–1091. <https://doi.org/10.1175/jpo3035.1>
- Dayan, H., Vialard, J., Izumo, T., & Lengaigne, M. (2014). Does sea surface temperature outside the tropical Pacific contribute to enhanced ENSO predictability? *Climate Dynamics*, *43*(5–6), 1311–1325. <https://doi.org/10.1007/s00382-013-1946-y>
- Dommenget, B. D., & Al-Ansari, M. (2022). Asymmetries in the ENSO phase space. *Climate Dynamics*, 1–20. <https://doi.org/10.1007/s00382-022-06392-0>
- Escoufier, R., & Robert, P. (1976). A unifying tool for linear multivariate statistical methods: The Rv-coefficient. *Applied Statistics*, *25*(3), 257–265. <https://doi.org/10.2307/2347233>
- Fedorov, A. V. (2010). Ocean response to wind variations, warm water volume, and simple models of ENSO in the low-frequency approximation. *Journal of Climate*, *23*(14), 3855–3873. <https://doi.org/10.1175/2010jcli3044.1>
- Graham, F. S., Brown, J. N., Wittenberg, A. T., & Holbrook, N. J. (2015). Reassessing conceptual models of ENSO. *Journal of Climate*, *28*(23), 9121–9142. <https://doi.org/10.1175/jcli-d-14-00812.1>
- Izumo, T., Lengaigne, M., Vialard, J., Luo, J. J., Yamagata, T., & Madec, G. (2014). Influence of Indian Ocean Dipole and Pacific recharge on following year's El Niño: Interdecadal robustness. *Climate Dynamics*, *42*(1–2), 291–310. <https://doi.org/10.1007/s00382-012-1628-1>
- Izumo, T., Lengaigne, M., Vialard, J., Suresh, I., & Planton, Y. (2018). On the physical interpretation of the lead relation between warm water volume and the El Niño southern oscillation. *Climate Dynamics*, *52*(5), 2923–2942. <https://doi.org/10.1007/s00382-018-4313-1>
- Izumo, T., Vialard, J., Dayan, H., Lengaigne, M., & Suresh, I. (2016). A simple estimation of equatorial Pacific response from windstress to untangle Indian Ocean Dipole and Basin influences on El Niño. *Climate Dynamics*, *46*(7–8), 2247–2268. <https://doi.org/10.1007/s00382-015-2700-4>
- Izumo, T., Vialard, J., Lengaigne, M., de Boyer Montegut, C., Behera, S. K., Luo, J. J., et al. (2010). Influence of the Indian Ocean Dipole on following year's El Niño. *Nature Geoscience*, *3*, 168–172. <https://doi.org/10.1038/ngeo760>
- Izumo, T., Vialard, J., Lengaigne, M., & Suresh, I. (2020). Relevance of relative sea surface temperature for tropical rainfall interannual variability. *Geophysical Research Letters*, *47*(3), e2019GL086182. <https://doi.org/10.1029/2019gl086182>
- Jin, F. F. (1997a). An equatorial ocean recharge paradigm for ENSO. Part I: Conceptual model. *Journal of the Atmospheric Sciences*, *54*(7), 811–829. [https://doi.org/10.1175/1520-0469\(1997\)054<0811:aeorpf>2.0.co;2](https://doi.org/10.1175/1520-0469(1997)054<0811:aeorpf>2.0.co;2)
- Jin, F. F. (1997b). An equatorial ocean recharge paradigm for ENSO. Part II: A stripped-down coupled model. *Journal of the Atmospheric Sciences*, *54*(7), 830–847. [https://doi.org/10.1175/1520-0469\(1997\)054<0830:aeorpf>2.0.co;2](https://doi.org/10.1175/1520-0469(1997)054<0830:aeorpf>2.0.co;2)
- Jin, F. F., Chen, H. C., Zhao, S., Hayashi, M., Karamperidou, C., Stuecker, M. F., et al. (2020). Simple ENSO models. In *El Niño Southern Oscillation in a changing climate* (pp. 119–151).
- Jourdain, N., Lengaigne, M., Vialard, J., Izumo, T., & Sen Gupta, A. (2016). Further insights on the influence of the Indian Ocean Dipole on the following year's ENSO from observations and CMIP5 models. *Journal of Climate*, *29*(2), 637–658. <https://doi.org/10.1175/JCLI-D-15-0481.1>
- Kessler, W. S. (2002). Is ENSO a cycle or a series of events? *Geophysical Research Letters*, *29*(23), 40–41. <https://doi.org/10.1029/2002gl015924>
- Lai, A. W. C., Herzog, M., & Graf, H. F. (2015). Two key parameters for the El Niño continuum: Zonal wind anomalies and Western Pacific sub-surface potential temperature. *Climate Dynamics*, *45*(11), 3461–3480. <https://doi.org/10.1007/s00382-015-2550-0>
- Linz, M., Tziperman, E., & MacMartin, D. G. (2014). Process-based analysis of climate model ENSO simulations: Intermodel consistency and compensating errors. *Journal of Geophysical Research*, *119*(12), 7396–7409. <https://doi.org/10.1002/2013JD021415>
- Masuda, S., Awaji, T., Toyoda, T., Shikama, Y., & Ishikawa, Y. (2009). Temporal evolution of the equatorial thermocline associated with the 1991–2006 ENSO. *Journal of Geophysical Research*, *114*(C3), C03015. <https://doi.org/10.1029/2008jc004953>
- McCreary, J. P. (1980). *Modelling wind-driven ocean circulation. JIMAR 80-0029, HIG 80-3*. p. 64. University of Hawaii. Honolulu.
- Meinen, C. S., & McPhaden, M. J. (2000). Observations of warm water volume changes in the equatorial Pacific and their relationship to El Niño and La Niña. *Journal of Climate*, *13*(20), 3551–3559. [https://doi.org/10.1175/1520-0442\(2000\)013<3551:ooowvc>2.0.co;2](https://doi.org/10.1175/1520-0442(2000)013<3551:ooowvc>2.0.co;2)
- Neelin, J. D., Battisti, D. S., Hirst, A. C., Jin, F. F., Wakata, Y., Yamagata, T., & Zebiak, S. E. (1998). ENSO theory. *Journal of Geophysical Research*, *103*(C7), 14261–14290. <https://doi.org/10.1029/97jc03424>
- Neske, S., & McGregor, S. (2018). Understanding the warm water volume precursor of ENSO events and its interdecadal variation. *Geophysical Research Letters*, *45*(3), 1577–1585. <https://doi.org/10.1002/2017GL076439>
- Petrova, D., Koopman, S. J., Ballester, J., & Rodó, X. (2017). Improving the long-lead predictability of El Niño using a novel forecasting scheme based on a dynamic components model. *Climate Dynamics*, *48*(3–4), 1249–1276. <https://doi.org/10.1007/s00382-016-3139-y>
- Ramesh, N., & Murtugudde, R. (2013). All flavours of El Niño have similar early subsurface origins. *Nature Climate Change*, *3*(1), 42–46. <https://doi.org/10.1038/nclimate1600>
- Santoso, A., Mcphaden, M. J., & Cai, W. (2017). The defining characteristics of ENSO extremes and the strong 2015/2016 El Niño. *Reviews of Geophysics*, *55*(4), 1079–1129. <https://doi.org/10.1002/2017rg000560>
- Suarez, M. J., & Schopf, P. S. (1988). A delayed action oscillator for ENSO. *Journal of the Atmospheric Sciences*, *45*(21), 3283–3287. [https://doi.org/10.1175/1520-0469\(1988\)045<3283:adaofe>2.0.co;2](https://doi.org/10.1175/1520-0469(1988)045<3283:adaofe>2.0.co;2)
- Takahashi, K., Montecinos, A., Goubanova, K., & Dewitte, B. (2011). ENSO regimes: Reinterpreting the canonical and modoki El Niño. *Geophysical Research Letters*, *38*(10), 1–5. <https://doi.org/10.1029/2011gl047364>
- Thual, S., Dewitte, B., Ayoub, N., & Thual, O. (2013). An asymptotic expansion for the recharge–discharge model of ENSO. *Journal of Physical Oceanography*, *43*(7), 1407–1416. <https://doi.org/10.1175/JPO-D-12-0161.1>
- Timmermann, A., An, S. I., Kug, J. S., Jin, F. F., Cai, W., Capotondi, A., et al. (2018). El Niño–southern oscillation complexity. *Nature*, *559*.
- Van Oldenborgh, G. J., Hendon, H., Stockdale, T., L'Heureux, M., De Perez, E. C., Singh, R., & Van Aalst, M. (2021). Defining El Niño indices in a warming climate. *Environmental Research Letters*, *16*(4), 044003. <https://doi.org/10.1088/1748-9326/abe9ed>
- Vijayeta, ., Dommenget, D., & McGregor, S. (2020). *ENSO in a changing climate simulations*. PhD thesis. Monash University.
- Wang, C., & Picaut, J. (2004). Understanding ENSO physics—A review. *Earth's Climate: The Ocean–Atmosphere Interaction, Geophys. Monogr.*, *147*, 21–48.
- Wyrtki, K. (1985). Water displacements in the Pacific and the Genesis of El Niño cycles. *Journal of Geophysical Research*, *90*(C4), 7129–7132. <https://doi.org/10.1029/jc090ic04p07129>
- Zhu, X., Greatbatch, R. J., & Claus, M. (2017). Interannual variability of tropical Pacific sea level from 1993 to 2014. *Journal of Geophysical Research: Oceans*, *122*(1), 602–616. <https://doi.org/10.1002/2016jc012347>

References From the Supporting Information

- An, S. I., Tziperman, E., Okumura, Y. M., & Li, T. (2020). ENSO irregularity and asymmetry. In *El Niño Southern Oscillation in a changing climate* (pp. 153–172).
- Ballester, J., Bordoni, S., Petrova, D., & Rodó, X. (2015). On the dynamical mechanisms explaining the western Pacific subsurface temperature buildup leading to ENSO events. *Geophysical Research Letters*, *42*(8), 2961–2967. <https://doi.org/10.1002/2015gl063701>
- Ballester, J., Bordoni, S., Petrova, D., & Rodó, X. (2016). Heat advection processes leading to El Niño events as depicted by an ensemble of ocean assimilation products. *Journal of Geophysical Research: Oceans*, *121*(6), 3710–3729. <https://doi.org/10.1002/2016jc011718>
- Bretherton, C. S., Widmann, M., Dymnikov, V. P., Wallace, J. M., & Bladé, I. (1999). The effective number of spatial degrees of freedom of a time-varying field. *Journal of Climate*, *12*(7), 1990–2009. [https://doi.org/10.1175/1520-0442\(1999\)012<1990:tenosd>2.0.co;2](https://doi.org/10.1175/1520-0442(1999)012<1990:tenosd>2.0.co;2)
- Capotondi, A., Wittenberg, A. T., Newman, M., Di Lorenzo, E., Yu, J. Y., Braconnot, P., et al. (2015). Understanding ENSO diversity. *Bulletin of the American Meteorological Society*, *96*(6), 921–938. <https://doi.org/10.1175/bams-d-13-00117.1>
- Cibot, C., Maisonnave, E., Terray, L., & Dewitte, B. (2005). Mechanisms of tropical Pacific interannual-to-decadal variability in the ARPEGE/ORCA global coupled model. *Climate Dynamics*, *24*(7), 823–842. <https://doi.org/10.1007/s00382-004-0513-y>
- Gadgil, S., Joseph, P. V., & Joshi, N. V. (1984). Ocean–atmosphere coupling over monsoon regions. *Nature*, *312*(5990), 141–143. <https://doi.org/10.1038/312141a0>
- Gasparin, F., & Roemmich, D. (2017). The seasonal march of the equatorial Pacific upper-ocean and its El Niño variability. *Progress in Oceanography*, *156*, 1–16. <https://doi.org/10.1016/j.pocean.2017.05.010>
- Hersbach, H., Bell, B., Berrisford, P., Hirahara, S., Horányi, A., Muñoz-Sabater, J., et al. (2020). The ERA5 global reanalysis. *Quarterly Journal of the Royal Meteorological Society*, *146*(730), 1999–2049. <https://doi.org/10.1002/qj.3803>
- Izumo, T. (2005). The equatorial undercurrent, meridional overturning circulation, and their roles in mass and heat exchanges during El Niño events in the tropical Pacific Ocean. *Ocean Dynamics*, *55*(2), 110–123. <https://doi.org/10.1007/s10236-005-0115-1>
- Izumo, T., Khodri, M., Lengaigne, M., & Suresh, I. (2018). A subsurface Indian Ocean dipole response to tropical volcanic eruptions. *Geophysical Research Letters*, *45*(17), 9150–9159. <https://doi.org/10.1029/2018gl078515>
- Jin, F.-F., Lin, L., Timmermann, A., & Zhao, J. (2007). Ensemble-mean dynamics of the ENSO recharge oscillator under state-dependent stochastic forcing. *Geophysical Research Letters*, *34*(3), L03807. <https://doi.org/10.1029/2006GL027372>
- Johnson, N. C., & Kosaka, Y. (2016). The impact of eastern equatorial Pacific convection on the diversity of boreal winter El Niño teleconnection patterns. *Climate Dynamics*, *47*(12), 3737–3765. <https://doi.org/10.1007/s00382-016-3039-1>
- Johnson, N. C., & Xie, S.-P. (2010). Changes in the sea surface temperature threshold for tropical convection. *Nature Geoscience*, *3*(12), 842–845. <https://doi.org/10.1038/ngeo1008>
- Khodri, M., Izumo, T., Vialard, J., Janicot, S., Cassou, C., Lengaigne, M., et al. (2017). Tropical explosive volcanic eruptions can trigger El Niño by cooling tropical Africa. *Nature Communications*, *8*(1), 1–13. <https://doi.org/10.1038/s41467-017-00755-6>
- Kumar, A., & Hu, Z. Z. (2014). Interannual and interdecadal variability of ocean temperature along the equatorial Pacific in conjunction with ENSO. *Climate Dynamics*, *42*(5), 1243–1258. <https://doi.org/10.1007/s00382-013-1721-0>
- McGregor, S., Ramesh, N., Spence, P., England, M. H., McPhaden, M. J., & Santoso, A. (2013). Meridional movement of wind anomalies during ENSO events and their role in event termination. *Geophysical Research Letters*, *40*(4), 749–754. <https://doi.org/10.1002/grl.50136>
- Okumura, Y. M. (2019). ENSO diversity from an atmospheric perspective. *Current Climate Change Reports*, *5*(3), 245–257. <https://doi.org/10.1007/s40641-019-00138-7>
- Palanisamy, H., Cazenave, A., Delcroix, T., & Meyssignac, B. (2015). Spatial trend patterns in the Pacific ocean sea level during the altimetry era: The contribution of thermocline depth change and internal climate variability. *Ocean Dynamics*, *65*(3), 341–356. <https://doi.org/10.1007/s10236-014-0805-7>
- Rayner, N. A., Parker, D. E., Horton, E. B., Folland, C. K., Alexander, L. V., Rowell, D. P., et al. (2003). Global analyses of sea surface temperature, sea ice, and night marine air temperature since the late 19th century. *Journal of Geophysical Research*, *108*(D14), 4407. <https://doi.org/10.1029/2002JD002670>
- Reynolds, R. W., Rayner, N. A., Smith, T. M., Stokes, D. C., & Wang, W. (2002). An improved in situ and satellite SST analysis for climate. *Journal of Climate*, *15*(13), 1609–1625. [https://doi.org/10.1175/1520-0442\(2002\)015<1609:aiaisas>2.0.co;2](https://doi.org/10.1175/1520-0442(2002)015<1609:aiaisas>2.0.co;2)
- Rebert, J. P., Donguy, J. R., Eldin, G., & Wyrski, K. (1985). Relations between sea level, thermocline depth, heat content, and dynamic height in the tropical Pacific Ocean. *Journal of Geophysical Research*, *90*(C6), 11719–11725. <https://doi.org/10.1029/jc090ic06p11719>
- Williams, I. N., & Patricola, C. M. (2018). Diversity of ENSO events unified by convective threshold Sea Surface temperature: A nonlinear ENSO index. *Geophysical Research Letters*, *45*(17), 9236–9244. <https://doi.org/10.1029/2018gl079203>
- Xie, P., & Arkin, P. A. (1997). Global precipitation: A 17-year monthly analysis based on gauge observations, satellite estimates, and numerical model outputs. *Bulletin of the American Meteorological Society*, *78*(11), 2539–2558. [https://doi.org/10.1175/1520-0477\(1997\)078<2539:gpayma>2.0.co;2](https://doi.org/10.1175/1520-0477(1997)078<2539:gpayma>2.0.co;2)
- Yokoi, T., Tozuka, T., & Yamagata, T. (2008). Seasonal variation of the Seychelles dome. *Journal of Climate*, *21*(15), 3740–3754. <https://doi.org/10.1175/2008jcli1957.1>
- Zuo, H., Balmaseda, M. A., Tietsche, S., Mogensen, K., & Mayer, M. (2019). The ECMWF operational ensemble reanalysis–analysis system for ocean and sea ice: A description of the system and assessment. *Ocean Science*, *15*(3), 779–808. <https://doi.org/10.5194/os-15-779-2019>